Spectroscopic Studies of Photoexcitations in Regioregular and Regiorandom Polythiophene Films**

By *XiaoMei Jiang*, *Ronald Österbacka*, *Oleg Korovyanko*, *Chong P. An*, *Baruch Horovitz*, *René A. J. Janssen*, and *Z. Valy Vardeny**

Using a variety of optical probe techniques we studied the steady state and transient dynamics of charged and neutral photoexcitations in thin films of poly-3-alkyl thiophene with regioregular order, which forms self-assembled lamellae structures with increased interchain interaction, as well as regiorandom order that keeps a chain-like morphology. In regiorandom polythiophene films we found that intrachain excitons with correlated photoinduced absorption and stimulated emission bands are the primary photoexcitations; they give rise to a moderately strong photoluminescence band, and long-lived triplet excitons and intrachain charged polarons. In regioregular polythiophene films, on the contrary we found that the primary photoexcitations are excitons with much larger interchain component; this results in lack of stimulated emission, vanishing intersystem crossing, and a very weak photoluminescence band. The long-lived photoexcitations in regioregular polythiophene films are interchain excitons and delocalized polarons (DP) within the lamellae, with very small relaxation energy. The characteristic properties of the DP species are thoroughly investigated as a function of the alkyl side group of the polymer backbone, film deposition conditions and solvents used, as well as at high hydrostatic pressure. The quantum interference between the low energy absorption band of the DP species and a series of photoinduced infrared active vibrations, which give rise to antiresonances that are superimposed on the electronic absorption band is studied and explained by a Fano-type interference mechanism, using the amplitude mode model.

1. Introduction

Interest in luminescent π-conjugated polymers (PCPs) has recently increased due to the potential optoelectronic applications including light-emitting diodes (LED), solar cells, and field-effect transistors (FET). The interest in PCPs attracted the 2000 Nobel prize in chemistry that was given to Heeger, McDiarmid, and Shirakawa. For many of their optoelectronic applications, the degree of structural order of the PCP active layer has been recognized as one of the key parameters governing the photophysics and consequently also its specific application for the optimal device performance. Whereas interchain interactions are usually detrimental for PCPs used in LEDs due to weak optical coupling to the ground state,[1] charge transport in the other applications requires good contacts between neighboring conjugated chains in the film. In addition, the traditional one-dimensional (1D) electronic structure in PCPs results in strong self-localization of the electronic excitations, which may also limit the carrier mobility to values of the order of 10^{-4} cm^2/volt s.[2]

Much higher mobilities, of the order of 0.1 cm^2/volt s have been recently obtained with regioregular substituted poly-3-hexyl thiophene (RR-P3HT) (Fig. 1b, inset) in FETs.[3] Such films were also successfully used in FETs to drive LEDs based on PCP, which demonstrated an all-organic display pixel.[4] Moreover, semiconductor to metal transition as well as superconductivity at a temperature of about 2.5 K have been recently demonstrated with RR-P3HT FET, where the carriers were injected into a thin polymer layer below the gate elec-

[*] Prof. Z. V. Vardeny, Dr. R. Österbacka,[+] Dr. O. Korovyanko, Dr. C. P. An, X. M. Jiang
Department of Physics, University of Utah
Salt Lake City, Utah 84112–0830 (USA)
E-mail: val@physics.utah.edu
Prof. B. Horowitz
Department of Physics, Ben Gurion University of the Negev
Beer-Sheva 84105 (Israel)
R. A. J. Janssen
Laboratory of Macromolecular and Organic Chemistry
Eindhoven University of Technology
NL-5600 MB Eindhoven (Netherlands)
[+] Second address: Department of Physics, Åbo Akademi University, Porthansgatan 3, FIN-20500 Turku, Finland.

[**] The work at the University of Utah was supported in part by the NSF DMR 02–02790 and DOE ER-45490. R. Ö. acknowledges funding from the Academy of Finland grant 48853.

  1616-301X/02/0909-0587 $ 17.50+.50/0

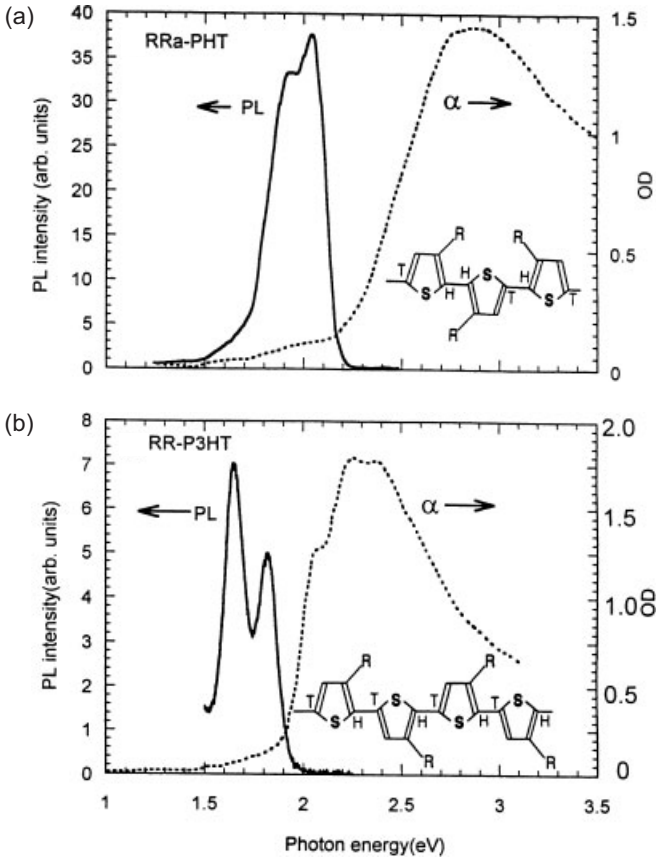

Fig. 1. The room-temperature absorption and photoluminescence spectra of RRa-P3HT (a) and RR-P3HT (b) films. The respective polymer regio-order structures are given in the insets. From Korovyanko et al. [8] with permission.

trode into the transport channel.[5] The reason for the dramatic increase in carrier mobilities is that self-organization of RR-P3HT chains results in a lamellae structure perpendicular to the film substrate.[3] In such lamellae two-dimensional (2D) sheets are formed having strong interchain interaction due to the short interchain interlayer distance of the order of 3.8 Å. Delocalization of the charge carrier among the lamellae has been invoked to be the reason for the high interlayer mobility. Recent optical studies of RR-P3HT films, where delocalized polaron excitations on adjacent chains have been measured using charge induced optical techniques in FETs,[3,6] as well as direct photogeneration in thin films,[7] have confirmed this assumption. On the contrary, P3HT films casted from polymer chains having regiorandom (RRa-) order (Fig. 1a, inset) form ordered lamellae to a lesser degree and the obtained field-effect carrier mobilities in FETs based on this polymer are consequently much smaller.[3] The main reason for the reduced carrier mobility is the lack of sufficiently strong interchain/interlamellae interaction that is caused by the chain-like film morphology.

In this work, we review our spectroscopic studies of the steady state[7] and transient[8] photoexcitation dynamics in films of RR-P3HT compared to those measured in films of RRa-P3HT. For these studies we have used a variety of optical techniques covering the time domains from 100 femtoseconds (fs) to 200 picoseconds (ps), as well as photomodulation and magneto-optical measurements under steady state conditions. We found that the photoexcitations in RRa-P3HT films are similar in many respects to those found in many other luminescent PCP films.[9–15] The primary photoexcitations in the ps time domain are intrachain excitons with correlated photoinduced absorption (PA) and non-overlapping stimulated emission (SE) bands. At longer times we identified long-lived triplet excitons with a near-infrared PA band, which are formed via intersystem crossing to the triplet manifold that competes with the moderately strong (8 % quantum efficiency) photoluminescence (PL) band. The long-lived charged photoexcitations in RRa-P3HT are intrachain polarons with two symmetric subgap PA bands, and a series of photoinduced infrared active vibrations (IRAVs). On the contrary, we found in RR-P3HT films that the primary photoexcitations are excitons with much larger interchain contribution. This leads to a weaker optical transition to the ground state that results in much weaker PL (< 0.5 %), lack of SE, and also to a vanishing intersystem crossing that prevents the formation of long-lived triplets. In addition, we also identified the precursor to polaron photogeneration in these films; these are geminate polaron pairs with ultrafast dynamics. The long-lived photoexcitations in RR-P3HT are delocalized polarons (DP), which have very small relaxation energy, as well as two asymmetric subgap PA bands, where the low energy band is red-shifted and much stronger compared to that of regular intrachain polarons. We found that the DP relaxation energy is intimately related to the film morphology; it can be easily changed using different solvents and

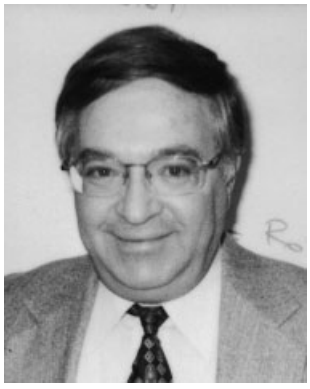

Z. Valy Vardeny has been on the Faculty in the Department of Physics, University of Utah since 1987, where he is a Distinguished Professor of Physics and Department Chair. Professor Vardeny has been involved in studying the optical properties of organic polymers, oligomers, and polyacenes in the form of films, high purity single crystals, and organic light-emitting diodes, as well as fullerenes and amorphous semiconductors. He has established the study of electronic and vibrational photoexcitation dynamics in organic and amorphous semiconductors from the femtosecond to the millisecond time domains, as well as in the steady state. For these measurements he uses ultrafast and cw lasers in a variety of spectroscopies, including optically detected magnetic resonance, laser action, nonlinear optical measurements, and pump-probe correlation techniques. He has published more than 400 papers on organic semiconductors and related research areas, and is named inventor on more than a dozen patents, patent applications, and patent disclosures.

  1616-301X/02/0909-0588 $ 17.50+.50/0 *Adv. Funct. Mater.* **2002**, *12*, No. 9, September

ADVANCED FUNCTIONAL MATERIALS

spin-cast conditions, as well as high hydrostatic pressure. The overlap between the PA band and the photoinduced IRAVs of the DP excitation in RR-P3HT results in quantum interference between the electronic and vibrational absorption bands that gives rise to a series of anti-resonances superimposed on the electronic PA. We explain these anti-resonances with a Fano-type model using the amplitude mode theory in the non-adiabatic approximation. We show that the photoinduced anti-resonances phenomenon exists in many ordered PCPs, and therefore is as generic as the photoinduced IRAVs with positive absorption lines.

2. Results and Discussion

The optical studies were performed using fs and ps transient spectroscopy as well as a variety of cw spectroscopies, on thin films of RR- and RRa-P3HT that were spin casted from solution. The time-resolved technique was the pump-probe correlation with 100 fs time resolution and spectral range from 1.1 eV to 2.2 eV, whereas the cw techniques include absorption, PL emission, PA and PA-detected magnetic resonance (PADMR) spectroscopies in the spectral range from 0.05 eV to 3.5 eV. These techniques are described in more detail in the experimental section attached at the end of this paper.

Figure 1 shows the absorption and PL spectra of RRa-P3HT and RR-P3HT films at room temperature.[8] The strong absorption band at photon energies over the energy-gap is due to π–π* transitions, and according to Kasha's rule, the PL emission comes from the lowest exciton in the system. We note the red shift of the RR-P3HT absorption and PL bands respect to those in RRa-P3HT, which is caused by the superior order in the lamellae structures.[3] The planar order leads to polymer chains with longer conjugations with fewer defects, such as twists and radicals on the chains. In addition, the absorption and the PL bands of the RR-P3HT film show pronounced structures due to phonon replica, indicating that the polymer chains in this film are more homogeneous than those in RR-P3HT films. In spite of the superior order, we measured in RR-P3HT an order of magnitude *decrease* in the PL quantum efficiency, η; in RRa-P3HT we measured $\eta \approx 8$ %, whereas in RR-P3HT we measured $\eta < 0.5$ %. The quantum efficiency decrease in RR-P3HT cannot be explained by an increase in the non-radiative decay rate, because this film contains fewer defects, and intersystem crossing to the triplet manifold is absent. We conjecture, therefore that the PL decrease in RR-P3HT is due to a weaker *radiative* transition of the lowest lying excitons in this film. Similar conclusion was also reached for excitons in RR-P3HT chains that form aggregates when dissolved in a poor solvent.[16] The weaker optical transition in the RR-P3HT films may be due to a larger interchain contribution for the lowest excitons in the lamellae compared to the usual intrachain excitons in RRa-P3HT. Indeed an interlayer separation of 3.8 Å in RR-P3HT lamellae causes a stronger interchain-interlayer interaction, as recently calculated using numerical quantum-chemical methods.[1,17] For an H-aggregate chain configuration this interaction leads to splitting of the HOMO and LUMO levels, so that the lower, red-shifted LUMO level becomes optically forbidden.[1] The weak PL that is still detected in RR-P3HT may be due to defects that are present in the film, which relax the optical selection rules. This model may explain the weak PL in RR-P3HT, as well as its red shift. The higher splitted LUMO level is optically allowed in this model,[1] and may be directly seen in absorption, which should be blue shifted respect to the PL. Hence from the Stokes shift of the 0–0 transition in absorption and PL spectra (Fig. 1b) we obtain an upper limit for the LUMO splitting in RR-P3HT of 250 meV,[18] in good agreement with recent model calculations.[1,17]

2.1. Femtosecond/Picosecond Spectroscopy

The fps dynamics studies in P3HT films with various regio-orders may further elucidate their excitons characteristic properties. Figure 2 shows the transient PA spectra of P3HT with both regio-orders measured at $t = 100$ fs and $t = 5$ ps, respectively following the pulse excitation.[8] The transient PA spectra of both films show two PA bands (PA_2 and PA_3), but only the fs spectrum of RRa-P3HT contains a SE band that is due to the photogenerated intrachain excitons. We explain the lack of SE in the RR-P3HT film as due to the much smaller oscillator strength for the photogenerated excitons in this material, confirming the above conclusion that the lowest lying excitons in RR-P3HT films are, in fact optically forbidden.

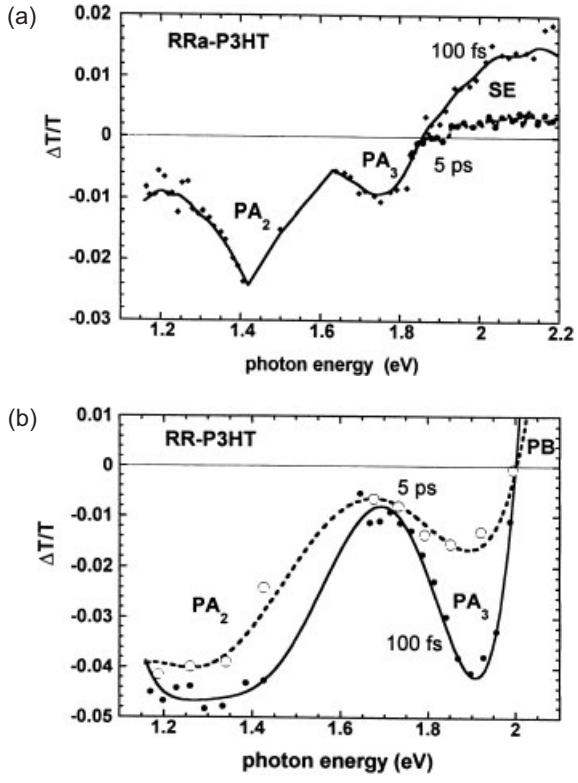

Fig. 2. The transient PA spectra of RRa-P3HT (a) and RR-P3HT (b) measured at 100 fs (full diamonds and circles) and 5 ps (full and empty circles), respectively following the pulse excitation. The PA, SE, and PB bands are assigned. From Korovyanko et al. [8] with permission.

  1616-301X/02/0909-0589 $ 17.50+.50/0

To better characterize the primary excitations in RRa-P3HT that are revealed in the ultrafast PA spectra, we studied the transient dynamics of each PA band and compared it with that of the SE band. Figure 3a[8] shows that the dynamics of PA_2 is similar to that of SE; both bands initially decay together, but the SE band disappears from the spectrum at 15 ps (Fig. 2a)

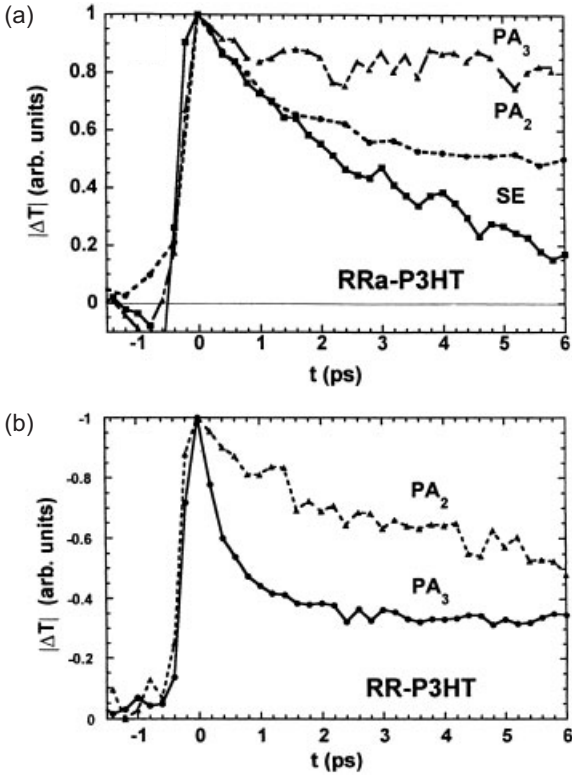

Fig. 3. Transient PA and SE decays in RRa-P3HT (a) and RR-P3HT (b), up to 6 ps. From Korovyanko et al. [8] with permission.

that is caused by the competing effect of PA_3. Due to their correlated dynamics at several different excitation intensities we conjecture that PA_2 and SE belong to the same species, namely intrachain excitons. Similar conclusion was drawn before for the correlated excitonic PA and SE in several other PCP films.[9–15] Moreover in some of the previous studies,[9,19] another correlated PA band (PA_1) was also detected in the near infrared (NIR) spectral range and was assigned to photogenerated excitons. In view of this, we anticipate that another excitonic PA band exists in RRa-P3HT in the near IR spectral range. This however will be confirmed in future studies.

On the contrary, PA_3 decay in RRa-P3HT is much slower than that of SE and PA_2 (Fig. 3a) and therefore, it does not involve intrachain excitons. In fact it decays only by a factor of about two from its initial, "$t = 0$" value within the maximum time delay of our apparatus (200 ps). We conjecture, therefore that PA_3 is due to interchain, trapped polaron pairs. Similar conclusion was drawn previously in ps studies of several other PCP films.[9–11] Such excitations may also be instantaneously generated onto two adjacent chains at a place on the chains close to their "contact-point", where the interchain distance is the smallest. Actually "contact points" may be also formed on the same chain between different chain segments, due to the chain molecular "cylindrical conformation" recently found in MEH-PPV using polarized PL.[20] This may explain the recent ps PA studies in some PPV-based PCP films, which were conducted in the mid IR spectral range (8–12 μm), where instantaneously generated infrared active vibrations (IRAV) were detected.[21,22] From this it was conjectured[22] that separated polarons are the primary excitations in PCP films. In view of our present results it is clear that in PCP films simultaneously with intrachain excitons, polaron pairs on adjacent chains or neighboring chain segments may be also generated. If the polarons reside on different chains or different segments of the same chain, then the polaron pair species can also give rise to IRAVs. However, as a result of the Coulomb attraction between the oppositely charged polarons, the polaron pair species are trapped near the "contact-point" of the adjacent chains (or neighboring segments) at which they had been originally generated, and thus would not contribute to transient photoconductivity. This may explain PA_3 slow dynamics.

We studied the transient dynamics of the two PA bands in the ps time domain also in RR-P3HT films (Fig. 3b).[8] As in RRa-P3HT films we also found that the ps transient decays of PA_2 and PA_3 in RR-P3HT films are not correlated. Moreover, the decay dynamics of PA_2 depends on the excitation intensity (I) showing faster decay at higher I that is perhaps due to exciton-exciton annihilation.[23] On the contrary, the decay dynamics of PA_3 is independent on (I). From this and the similarity with the PA transient spectrum in RRa-P3HT discussed above, we conclude that PA_2 and PA_3 in RR-P3HT are, likewise due to excitons and geminate polaron pairs, respectively. The lack of fs SE band in RR-P3HT shows that the primary photoexcitations in the lamellae are not regular intrachain excitons. This may explain the reason why the excitonic PA band in this film, namely PA_2 (Fig. 2b) is much broader than that in RRa-P3HT (Fig. 2a). The observed broadening may be due to the splitting of the even parity states (A_g) that are optically coupled to the lower lying excitons (or "$1B_u^-$"). Similar as for the LUMO level[1] these A_g states may also split due to the increased interlayer interchain coupling in the lamellae that causes excess broadening of their optical transitions.

The band PA_3 in RR-P3HT (Fig. 2b) is substantially stronger than that in RRa-P3HT (Fig. 2a). This shows that the polaron pair generation process is more efficient in RR-P3HT films. This is not surprising since the polymer chains in the lamellae are longer and closer to each other, so that the "contact-points" between any two adjacent chains in two neighboring lamellae layers are therefore more extended. Moreover, the extended "contact-points" for the polymer chains in adjacent lamellae leads to a more mobile polaron pair species in RR-P3HT compared to that in RRa-P3HT. The higher polaron pair mobility results in a faster PA_3 decay in RR-P3HT (Fig. 3b) compared to that in RRa-P3HT (Fig. 3a). We could fit PA_3 transient decay in RR-P3HT with a two-component decay function;[8] a fast component using a $t^{-1/2}$ decay with a 0.5 ps lifetime, and a slow component. The $t^{-1/2}$ decay that we found for the geminate polaron pair in RR-P3HT is in agreement with the diffusion-limited geminate recombination considered

  1616-301X/02/0909-0590 $ 17.50+.50/0 *Adv. Funct. Mater.* **2002**, *12*, No. 9, September

ADVANCED FUNCTIONAL MATERIALS

before for the photogenerated geminate soliton-antisoliton pair recombination in trans polyacetylene [*t*–$(CH)_x$].[24] Similar as in RRa-P3HT, the slow PA_3 component in RR-P3HT decays only slightly during the 200 ps time interval of our measurements. We interpret the two respective PA_3 decay components as polaron pairs that are generated in the lamellae, which are more mobile and consequently have faster dynamics; and polaron pairs that are generated in the disordered portions of the polymer film, where the lamellae are not perfect. The latter polaron pair excitations, similarly as in RRa-P3HT are less mobile and consequently have slower dynamics.

2.2. Steady State Spectroscopy

The *long-lived* photoexcitations in the P3HT films with different regio-orders were studied by cw PA and PADMR spectroscopies. These spectroscopies are based on a standard photomodulation [PM] set-up, and a FTIR spectrometer. The PM set-up is sensitive to photoexcitations having lifetime, $\tau < (2\pi f)^{-1}$, where f is the modulation frequency of the laser beam. On the contrary, the FTIR PM set up mainly shows very long-lived photoexcitations with τ of the order of a second or longer.

2.2.1. RRa P3HT

Figure 4b shows that a strong PA band, T_1 at 1.45 eV dominates the PM spectrum in RRa-P3HT films.[7] At larger amplification (×30) we also observed a PA band P_1 at 0.5 eV. This band is correlated with a series of narrow lines below about 200 meV that are considered to be IRAVs, which are made IR-active due to the induced charges on the chains. The two PA bands have different dynamics as measured by their distinctive different dependencies on the laser excitation intensity (I), and modulation frequency (f). Whereas the band T_1 has a linear I dependence and a well defined lifetime (of about 1 ms), the band P_1, in contrast has a sublinear I dependence, and does not have a unique lifetime. Actually it has a wide distribution of lifetimes ranging from a few ms to a few seconds. We conclude, therefore that the two PA bands are due to two different types of photoexcitations. Similar PA bands have been found in many other PCP and are thus very well understood. The T_1 band is due to a strong optical transition in the triplet manifold that is from the lowest lying triplet into the continuum band, and is therefore a signature of triplet excitons. For this assignment we have strong experimental evidence using the PADMR technique.

We measured (Fig. 5a) the λ-PADMR spectrum at resonant magnetic field, $H_{1/2} = 430$ G corresponding to $g \approx 5.1$, which is due to microwave transitions between two triplet sublevels with a substantial zero-field splitting (dubbed "half-field"[25]). We found[26] that the PADMR spectrum contains a single negative ΔT band at 1.45 eV, which is similar to the PA spectrum. This unambiguously shows that the band T_1 is due to triplet

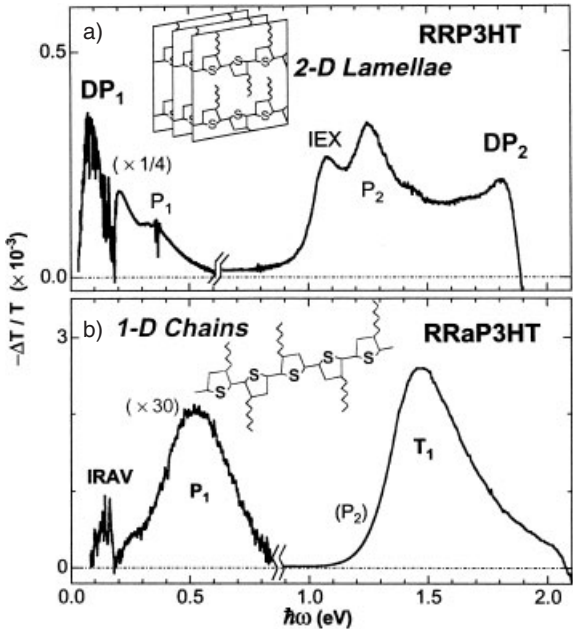

Fig. 4. Cw PA spectra of RR-P3HT (a) and RRa-P3HT (b) at 80 K. Various PA bands are introduced where DP_1 and DP_2 are for delocalized polarons, P_1 and P_2 are for intrachain polarons, IEX is interchain excitons and T_1 is for the triplet excitons. The lamellae and isolated P3HT chains are also shown in the insets. From Österbacka et al. [7] with permission.

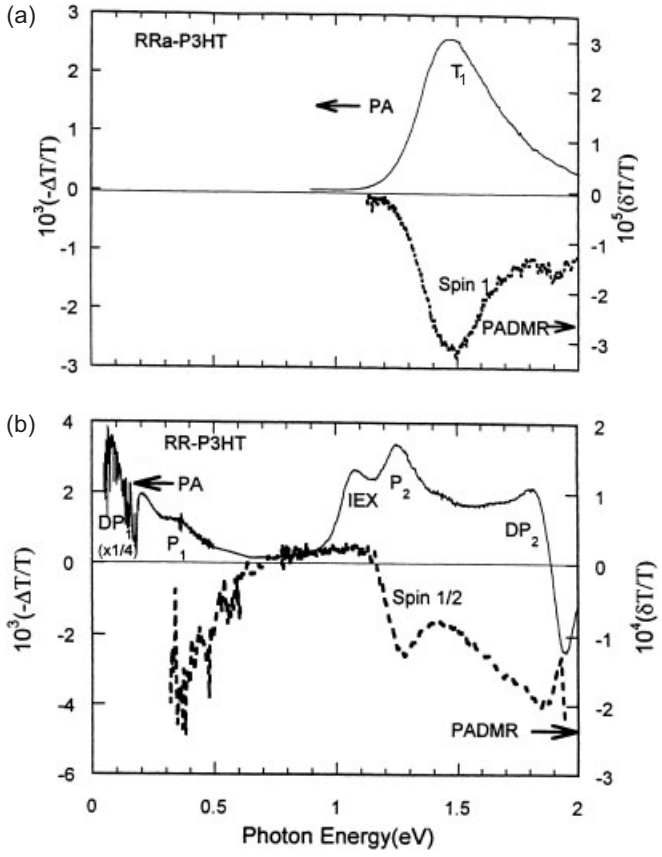

Fig. 5. Cw PA and λ-PADMR spectra of RRa-P3HT (a) and RR-P3HT (b) films measured at 10 K. The λ-PADMR in (a) was measured at $H_{1/2} = 430$ G, which corresponds to transitions among spin 1 triplet sublevels at $g \approx 5.1$, whereas in (b) it was measured at $H = 1006$ G, which corresponds to transitions among spin 1/2 doublet sublevels at $g \approx 2$. Several PA bands are assigned. From Korovyanko et al. [8] with permission.

  1616-301X/02/0909-0591 $ 17.50+.50/0

excitons. The long-lived triplets are formed via intersystem crossing to the triplet manifold with a time constant longer than our ps measurements limit of 200 ps. In fact typical intersystem crossing time in PCP films were determined to be of the order of 5 ns.[27] This long decay time would not be seen in our ps transient measurements.

In addition to the band T_1 we also measured a weak PA band (P_1) in the mid IR spectral range. The PA band P_1 is the low energy absorption band of intrachain polarons (Fig. 4b), and its correlation with the photoinduced IRAVs shows that the underlying photogenerated species are indeed charged. The higher polaron band (P_2) should appear in the vis-NIR spectral range, but is not observed here. This happens since the much stronger band T_1 in the PM spectrum probably overshadows it.

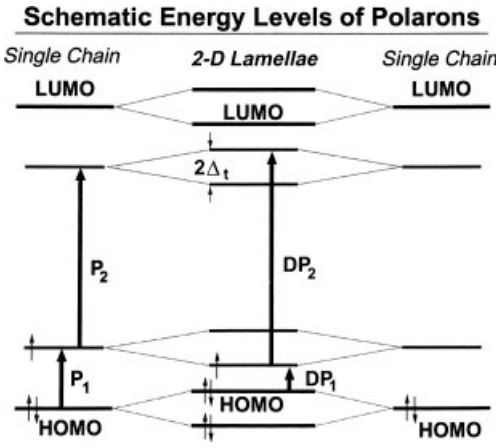

Fig. 6. The model for the gap energy levels and related allowed optical transitions of intrachain polarons and delocalized polaron excitations. $2\Delta_t$ is the DP level splitting and the relation $E(DP_1) + E(DP_2) = E(P_1) + E(P_2)$ holds.

2.2.2. RR-P3HT

The cw PA spectrum of RR-P3HT films (Fig. 4a) is much richer.[7] It contains two PA bands DP_1 at 0.1 eV and DP_2 at 1.8 eV, respectively that are due to 2D delocalized polarons in the lamellae (Fig. 6),[3,6–7] as well as PA bands P_1 at 0.35 eV and P_2 at 1.25 eV, respectively that are due to localized intrachain polarons in the disordered portions of the film.[7] In agreement with this assignment the two DP bands have the same dynamics; also the two P bands have the same dynamics, which is not correlated to those of the DP bands. We note that DP_1 is red-shifted respect to P_1, whereas DP_2 is blue-shifted respect to P_2. Moreover the sum rule: $E(DP_1) + E(DP_2) = E(P_1) + E(P_2)$ approximately holds.[7,26] An interaction model depicted in Figure 6 explains both the energy shift of the DP bands respect to the P bands, and the experimentally demonstrated sum rule. In this model the strong interchain interaction of the DP species splits the two intrachain polaron levels in the gap in such a way that the lower (upper) optical transition becomes optically allowed. Another feature in the PM spectrum (Fig. 4a) is a PA band dubbed IEX at 1.1 eV that was tentatively identified[7,26] as due to trapped interchain singlet excitons in the lamellae.

The λ-PADMR spectrum measured in RR-P3HT at resonant field that corresponds to $g \approx 2$ due to spin 1/2 carriers is shown in Fig. 5b,[8] and confirms the previous assignments of the various PA bands.[7] This spectrum shows that, except for the IEX band, all other PA bands in the PM spectrum are associated with spin 1/2 carriers. In particular DP_2, which spectrally overlaps with PA_3 in the ps transient spectrum (Fig. 2b), may be now associated with spin 1/2 polarons. This indicates that PA_3 in RR-P3HT is a precursor to the formation of long-lived polarons in the film, in agreement with its assignment in the transient spectra above. In fact the band DP_2 may be due to the long-lived tail of the species associated with PA_3 in the ps time domain. It is also seen in Fig. 5b that IEX is not associated with any spin 1/2 excitation, in agreement with its previous assignment[26] that it results from trapped spin *singlet* excitons. We note that IEX spectrally overlaps with PA_2 (Fig. 2b) indicating that these two bands, in fact belong to the same species; except that the IEX represents the long-lived tail of the photogenerated excitons associated with PA_3.

Using PADMR at $H_{1/2}$ that corresponds to $g \approx 5.1$ of triplet species,[8] long-lived spin 1 excitations *have not* been found in RR-P3HT films. This shows that long-lived triplet excitons are not easily generated in RR-P3HT lamellae. In RR-P3HT solutions, on the contrary long-lived photogenerated triplets do exist, and an intersystem crossing (ISC) time constant of about 5 ns was determined.[27] We therefore conjecture that the delocalized interchain interlayer excitons in the lamellae do not easily turn into localized intrachain triplet excitons in RR-P3HT via ISC. This is another strong evidence that the primary photoexcitations in RR-P3HT are not the ordinary intrachain excitons, as found in many other PCP films. Instead, they are delocalized among adjacent layers, similar to the delocalized polarons in the lamellae studied before,[3,6–7] with a consequent suppression of ISC into the triplet manifold. We note that ISC suppression was also observed recently in aggregates of long oligo-thiophenes below the aggregate formation temperature.[28] ISC suppression might therefore be a general consequence of enhanced interchain interaction.

3. The Polaron Relaxation Energy

Polaron excitations in PCPs have two correlated optical bands below the gap;[29] these are P_1 in the mid-infrared and P_2 in the near-infrared spectral range (Fig. 7, inset). P_1 for a positive polaron is an optical transition from the HOMO band into the lower polaron ingap level, whereas for a negative polaron it is a transition between the upper polaron ingap level into the LUMO band; P_1 is thus directly related to the polaron relaxation energy, E_r. P_2, on the contrary is the optical transition between the two polaron levels inside the gap and is thus related to the separation between them[29] (Fig. 7, inset).

Figure 7[30] shows the PA spectra of two regioregular poly(3-alkyl-thiophene) [P3 AT] that were measured at 20 K; one is RR-P3HT (Fig. 7a) and the other is RR-P3 AT that has a very long alkyl side group (Fig. 7b). We note that whereas RR-P3HT forms lamellae in the film,[3] the second polymer chains

  1616-301X/02/0909-0592 $ 17.50+.50/0 Adv. Funct. Mater. 2002, 12, No. 9, September

ADVANCED FUNCTIONAL MATERIALS

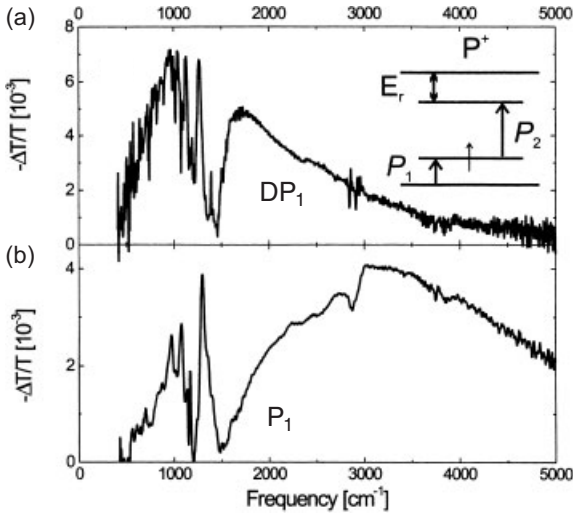

Fig. 7. PA spectra in the mid-IR spectral range for films of RR-P3HT (a) and RR-P3 AT with long attached alkyl side group (b). The inset schematically shows the two polaron levels in the gap and associated optical transitions, where the polaron relaxation energy is defined. From Österbacka et al. [30] with permission.

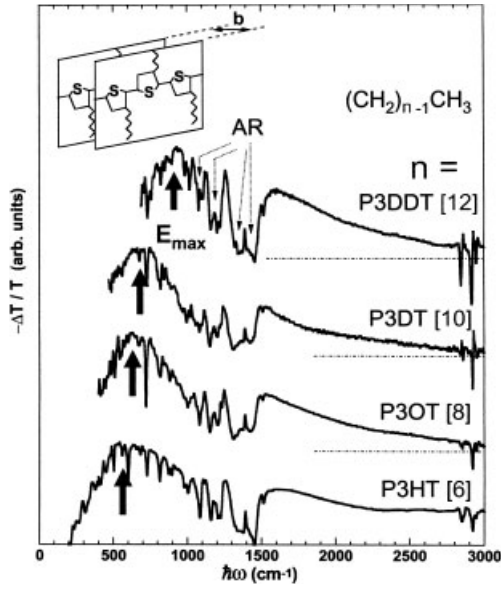

Fig. 8. The DP_1 PA band in RR-P3 AT films for alkyl side chains $(CH_2)_{n-1}CH_3$ of various length n. The antiresonances (ARs) features are assigned and the maximum energy E_{max} in DP_1 for each polymer chain is marked by an arrow. From Österbacka et al. [7] with permission.

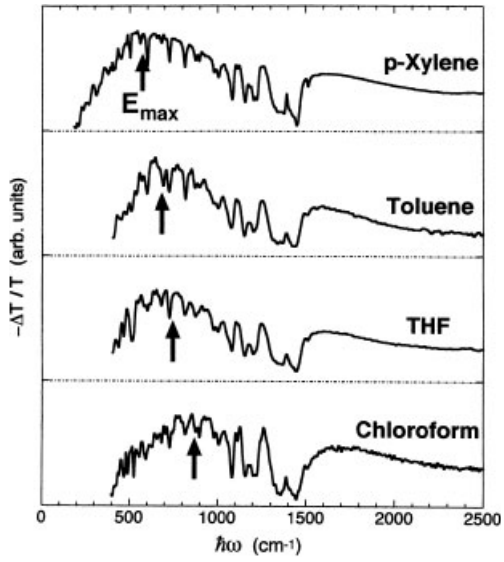

Fig. 9. The DP_1 PA band in RR-P3HT films casted from solutions of different solvents. E_{max} for the various DP_1 bands are marked with arrows. From Jiang et al. [31] with permission.

do not form lamellae because of the very long attached side group. One of the pronounced differences between the two PA spectra in Figure 7 is the PA band marked DP_1 and P_1; in RR-P3HT DP_1 peaks at about 1000 cm^{-1} (Fig. 7a), and is due to the DP species,[7] whereas P_1 peaks at about 3000 cm^{-1} in the less ordered polymer film (Fig. 7b) and is due to intrachain polarons, similar to the case of RRa-P3HT discussed above. We therefore conclude that the polaron relaxation energy, E_r is substantially smaller in the more ordered film.

In fact, the peak, E_{max} of the DP_1 band is very sensitive indicator for the polaron relaxation energy and thus can be closely monitored to study the film morphology. We assume that E_r is smaller the more ordered are the polymer chains in the film; this is caused by the stiffer environment in the ordered films. For example, the size of the alkyl size group may determine E_r in RR-P3 AT films through the chain stiffness. In Figure 8 we show the DP_1 band in several P3 AT films, $(CH_2)_{n-1}CH_3$ with $n = 6$ to $n = 12$.[7] It is seen that DP_1 blue shifts as n increases, indicating that larger polaron relaxation occurs in lamellae formed with P3 AT with larger side group. One explanation for the larger E_r with n is the increase of the interlayer distance b with n[7] as depicted in Figure 8 inset. In fact, very long side groups destroy lamellae formation as for the P3 AT film shown in Figure 7b.

Different solvents may also play an important role in controlling the interchain interaction, which in turn controls lamellae formation in the film. The order and size of the lamellae determine E_r, and therefore RR-P3HT films spun from different solvents may show slightly different E_{max} for the DP_1 band. This is shown in Figure 9, where the obtained DP_1 band in films spun from different solvents is depicted.[31] It is seen that films prepared from solution of solvents with high boiling temperatures, T_B such as *p*-xylene ($T_B = 138\,°C$) has a lower E_{max} compared with that of films prepared with solvents of low T_B such as chloroform ($T_B = 61°C$).[31] Bao et al. have found in their FET fabrication made of RR-P3HT polymers that the film quality and field-effect mobility are strongly correlated with the choice of solvents.[32] Also in the ps work of Nguyen et al.[33] it has been shown that the PCP film morphology changes with the solvent and spin casting speed. Similarly, the RR-P3HT polymer chains in our case are probably more planar and neatly arranged in *p*-xylene solutions, resulting in more ordered lamellae and consequently smaller polaron relaxation. On the contrary, the RR-P3HT chains tend to be more coiled in chloroform solutions, thus the lamellae in films casted from this solvent are less ordered, and consequently E_r is larger.

High hydrostatic pressure may also influence the properties of the DP species. The interlayer distance b may decrease at

  1616-301X/02/0909-0593 $ 17.50+.50/0

high pressures thus directly influencing E_r. High hydrostatic pressure may also increase the chain stiffness further reducing E_r. We have devised an IR PM set-up at high hydrostatic pressures using the FTIR spectrometer. It is based on a diamond anvil cell, where the pressure is calibrated by the shift of the IR active C–H stretching vibration frequency in the polymer chain. Figure 10 compares the DP_1 PA band in RR-P3HT obtained at 30 Kbar and ambient pressures. It is seen that the sharp features related to the photoinduced IRAVs blue shift at high pressures, which is usually the case for vibrational lines. Although it is difficult to observe a shift in E_{max} at high pressure, still the overall shift in the DP_1 PA band is to *lower* energies. This may be quantitatively observed when the DP_1 band is fit using a 2D model (Fig. 10). At the higher pressure it is easy to see that the low-energy tail of DP_1 increases, whereas the high-energy shoulder decreases. These changes indicate that indeed the DP species becomes even more delocalized at high hydrostatic pressure, presumably because the increase in the interchain interlayer interaction.

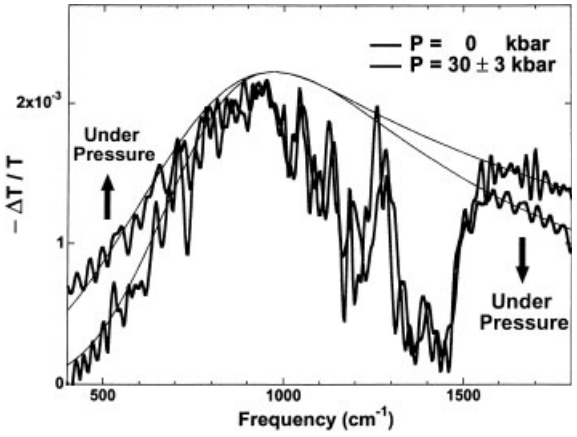

Fig. 10. The DP_1 PA band in RR-P3HT film at ambient pressure and high hydrostatic pressure of 30 kbar. The solid smooth lines are fits to the electronic PA bands emphasizing its red shift at high pressure; note the sharp ARs blue shift at high pressure.

4. The Spectral Antiresonances

The most striking difference between the two PA spectra illustrated in Figure 7 is the sharp photoinduced features at frequencies below about 1600 cm^{-1} that are due to photoinduced IRAVs. Whereas in the less ordered film the photoinduced IRAVs appear as positive absorption lines (Fig. 7b), they appear as dips, or anti-resonances (AR) superimposed on the DP_1 PA band in the ordered film (Fig. 7a).[7] These AR dips are apparently caused by the overlap between the IRAV lines and the DP_1 band. Moreover, the AR spectrum (Fig. 7a) contains much sharper dips and consequently is much richer than the positive photoinduced IRAV spectrum.

Photoinduced AR lines are not unique to RR-P3HT, which happens to form lamellae in the casted films.[3] In fact we found that ARs are quite a generic phenomenon in ordered films, where the polaron P_1 band overlap with the IRAVs. Figures 11a to d shows the PA spectra of several other ordered polymer films.[30] In all of them photoinduced ARs superimposed on P_1 are apparent. In some polymers the separation between positive IRAVs and negative ARs is difficult, especially where the overlap with the P_1 band is less pronounced (Figs. 11a to c). We also note that in PPE there exists a prominent AR at much higher frequency (at about 2100 cm^{-1}) than in the other polymers, which is probably related to the modified C≡C triple bond stretching vibration associated with this polymer chain. We also note that the literature contains other examples of photoinduced ARs in the PA spectra, such as in polydiacetylene single crystals,[34] for example, and other polymer films where the AR phenomenon was not recognized.[35] We conclude that photoinduced ARs are as common as photoinduced positive IRAVs and therefore an appropriate model to describe them is in order here.

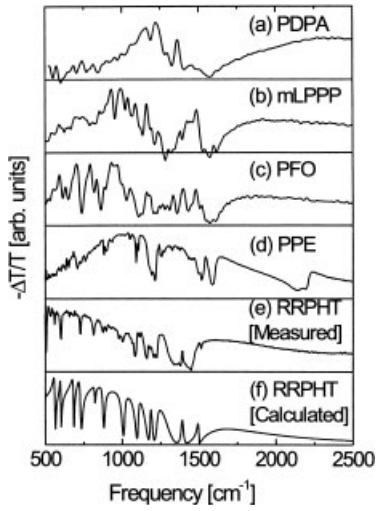

Fig. 11. PA spectra in the mid-IR spectral range in various ordered PCP films. In (f) the calculated spectrum for RR-P3HT is shown (see text), and compared to the data (e). From Österbacka et al. [30] with permission.

We analyze the AR spectrum using the amplitude mode (AM) model,[36,37] which has had spectacular success in explaining the resonant Raman scattering (RRS) dispersion as well as photoinduced and doping induced IRAVs in PCP.[37] In all of these previous applications of the AM model it has been explicitly assumed that the adiabatic approximation holds true. This was correct since the Raman line frequencies are much smaller than the optical gap, and the IRAV frequencies were much smaller that the energy of the photoinduced or doping-induced electronic bands. This approximation, however, does not hold in our case since the IR-active lines overlap with the electronic transition; we thus modified the AM model to include the non-adiabatic limit.[30] In this case, we took into account both vibronic and electronic transitions, as well as the quantum interference between the two types of photoexcitations.

An important ingredient of the AM model is that all IRAVs are interconnected and contribute to the same phonon propagator.[37] This case is unique to ARs in polymers, and substantially differs from the more regular Fano-type resonance treatments in

  1616-301X/02/0909-0594 $ 17.50+.50/0 *Adv. Funct. Mater.* **2002**, *12*, No. 9, September

ADVANCED FUNCTIONAL MATERIALS

other materials.[38–42] We therefore start by defining the pinned, many-phonon-propagator, $D_\alpha(\omega) = D_0(\omega)/[1-\alpha_p-D_0(\omega)]$, where α_p is the polaron-vibrational pinning parameter and $D_0(\omega)$ is the bare phonon propagator. The latter is given[36] by: $D_0(\omega) = \sum_n d_{0,n}(\omega)$, and $d_{0,n}(\omega) = \lambda_n/\lambda\{(\omega_n{}^0)^2/[\omega^2-(\omega_n{}^0)^2-i\delta_n]\}$, where $\omega_n{}^0$, δ_n, and λ_n are the bare phonon frequencies, their natural linewidth (inverse lifetime) and electron–phonon (e–p) coupling constant, respectively, and $\sum\lambda_n = \lambda$, which is the total e–p coupling. In the non-adiabatic limit, for a polaron current coupling to phonons, $f(\omega)$ that influences the conductivity, $\sigma(\omega)$ (and hence also shows up in the absorption spectrum, since imaginary(σ) $\approx \alpha$), there is a correlated contribution, $g(\omega)$ from the most strongly coupled phonons via the e–p coupling. The function $g(\omega)$ is given in the random phase (RPA) approximation by:[43,44]

$$g(\omega) = \omega^2/E_r{}^2[-\lambda D_\alpha(\omega)f^2(\omega)]/[1+2\lambda D_\alpha(\omega)\Pi_\varphi(\omega)] \quad (1)$$

where $\Pi_\varphi(\omega)$ is the phonon self mass correction due to the electrons, which can be approximated for charge density wave (CDW) by the relation:

$$2\lambda\Pi_\varphi(\omega) = 1 + c(\omega) \quad (2)$$

In the CDW approximation $c(\omega)$ is given by:

$$c(\omega) = \lambda\omega^2 f(\omega)/E_r{}^2 \quad (3)$$

but since for $\omega > E_r$, $f(\omega)$ changes slowly over the phonon linewidth, we may take it to be a constant, C. The RPA terms in Equation 1 contain the sharp structure of $D_\alpha(\omega)$, whereas additional non RPA terms contribute a smooth background term.

In general the conductivity spectrum, $\sigma(\omega)$ is given by[44]

$$\sigma(\omega) = (\omega_p{}^2/4\pi i\omega)[d(\omega) + g(\omega) - 1] \quad (4)$$

where ω_p is the plasma frequency, which is proportional to the photoinduced carrier density, and $[d(\omega) - 1]$ is the response in the absence of phonons that also includes non RPA terms. In the CDW approximation $d(\omega) = f(\omega)$.[45] Hence the sharp structure of Equation 4 can be written as

$$\sigma(\omega) \approx [1 + D_0(\omega)(1-\alpha')]/[1+D_0(\omega)(1+C-\alpha)] \quad (5)$$

where α' is a constant that replaces a smooth electronic response; in the CDW approximation[45] we have $\alpha' = \alpha_p$, which was defined above for the trapped polaron excitation.

The poles of Equation 5, which can be found from the relation: $D(\omega) = -(1-\alpha_p + C)^{-1}$, give peaks (or IRAVs) in the conductivity (absorption) spectrum. On the other hand, the zeros in Equation 5, which can be found by the relation: $D_0(\omega) = -(1-\alpha_p)^{-1}$, give the indentations (or ARs) in the conductivity (absorption) spectrum. It is thus apparent that the ARs are due to the formation of quantum interference between the phonons and the electron optical transitions in the conductivity spectrum.

To see the effect of the non-adiabatic limit on the PA spectrum we calculated[30] the conductivity spectrum, including the IRAVs for polarons with both low and high E_r, as seen in Figure 12. For these calculations we used the phonon parameters of RR-P3HT[46] with 13 strongly coupled vibrational modes and approximated the electronic band contribution, $f(\omega)$, by

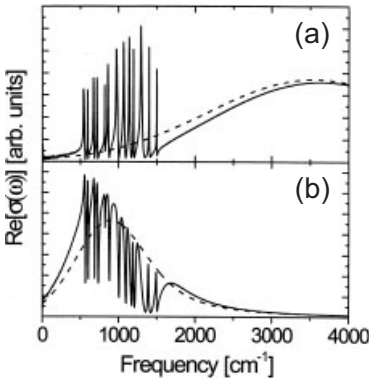

Fig. 12. Calculated PA spectra (solid lines) using the CDW response function $f(\omega)$ [45] (broken lines) with onset 2Δ at: a) $2\Delta = 3600$ cm^{-1} and FWHM of 2400 cm^{-1}, b) FWHM and $2\Delta = 800$ cm^{-1}. From Österbacka et al. [30] with permission.

the CDW response function,[45] where the CDW gap $2\Delta = E_r$, and E_r is associated with the polaron relaxation energy that governs the P_1 band. It is seen that when $\omega \ll E_r$, then only IRAVs with positive peaks can be observed (Fig. 12a); this happens since C in Equation 3 is negligible small, and consequently ARs are not formed. However, when E_r is small so that the CDW band overlaps with the IRAVs, then quantum interference occur that gives rise to ARs in the spectrum (Fig. 12b); in this case the ARs are more dominant than the IRAVs that occur on their high energy side. We note the qualitative similarity of the experimental data (Fig. 7a) with the model (Fig. 12b), which shows that our approach catches the essence of the ARs phenomenon.

To have a more quantitative fit to the experimental PA spectrum of RR-P3HT we used both resonant Raman scattering (RRS) and doping induced absorption spectra of this polymer film to determine the 13 bare phonon frequencies and their corresponding e–p couplings.[30,46] The advantage of using the AM model is that the same phonon propagator, $D_0(\omega)$, which determines the photoinduced AR and IRAV frequencies, also determines the RRS and doping induced IRAV frequencies.[37] The RRS frequencies are the solution of the equation: $D_0(\omega) = -(1-2\tilde{\lambda})^{-1}$, where $\tilde{\lambda}$ is the effective e–p coupling, whereas the doping induced IRAV frequencies are correspondingly given by the equation: $D_0(\omega) = -(1-\alpha_{p'})^{-1}$, where $\alpha_{p'}$ is the pinning parameter associated with the doping-induced polarons.[36] The obtained phonon parameters of RR-P3HT have been published before[30,46] and were used to calculate, via the AM model, the doping induced IRAV, RRS and photoinduced IRAV and AR frequencies.[30]

The actual fit to the RR-P3HT photoinduced ARs *spectrum* is seen in Figure 11f and can be compared with the measured spectrum (Fig. 11e). The excellent agreement between theory and experiment was obtained by using the CDW absorption band[45] to represent the polaron P_1 band with $E_r = 2\Delta = 900$ cm^{-1}. For this fit a distribution in 2Δ of about 60 % and a distribution in α

  1616-301X/02/0909-0595 $ 17.50+.50/0

of 12 % around $\alpha = 0.38$, with $C = -0.08$ was necessary. The disorder and inhomogeneity that still exist in RR-P3HT films in spite of the lamella formation justify the parameter distributions.

In view of the excellent agreement between theory and experiment that is seen in Figure 11e and f, we conjecture that the AM model and a continuum electronic band for P_1 such as the CDW, can quantitatively describe the AR phenomenon in ordered PCP films. This conclusion strongly indicates that the photoinduced polaron band in such materials is *continuous*. Since the polaron PA band involves optical transitions between a localized level in the gap and the HOMO or LUMO levels in the charge manifold of these polymers (Fig. 7, inset), we conclude that these levels in ordered polymers are, in fact *continuous bands*.[47,48] In such bands electrons can be readily accelerated due to external forces, as in inorganic semiconductors, and thus the treatments of ordered polymers in OLEDs and FETs via band bending to form depletion and accumulation layers[49] as in more regular semiconductors are, a-posteriori justified.

5. Summary and Conclusions

In this work, we reviewed the optical properties of P3 AT polymer films with two regio-orders, namely regioregular that forms lamellae in spin-cast films, and regioregular that forms lamellae to a lesser degree. The photoexcitations in films casted from solutions of these two polymers are very different from each other because of the different film morphologies that influence the interchain interaction. In RRa-P3HT we found that intrachain excitons are the primary photoexcitations, which give rise to a prominent PL band with about 8 % quantum efficiency; these properties are similar to many other PCP films, where the polymer chains are isolated from each other. The intrachain singlet excitons show SE and PA bands that do not overlap and therefore RRa-P3HT can be used to obtain laser action in neat films. In the nanosecond time domain there is substantial intersystem crossing to the triplet manifold and this gives rise to long-lived triplet excitons. A tiny portion of the intrachain excitons separates into polaron pairs and later into isolated, long-lived intrachain polarons. These intrachain polarons show two subgap absorption bands with approximately equal intensity, which are correlated with IRAVs having positive absorption lines.

In contrast to RRa-P3HT, the primary photoexcitations in RR-P3HT films are delocalized among neighboring lamellae layers in the film. Thus, in this case the photogenerated excitons have larger interchain component and this reduces the PL strength by an order of magnitude, to less than 0.5 %, and this does not allow a SE band to appear in the fs time domain. The interlayer interchain excitons cross to the triplet manifold to a lesser degree and thus long-lived triplet excitons are not observed in RR-P3HT films. Because the enhanced interchain character in RR-P3HT the excitons may dissociate more into polaron pairs, which later separate into isolated polarons. Similar to the excitons in the ps time domain, the long-lived charged polarons in RR-P3 AT are also delocalized among adjacent lamellae forming delocalized polaron (DP) excitations. The DPs also show two subgap PA bands, but they are shifted respect to those of isolated polarons, and their intensity is quite asymmetric; in this case the lower energy PA band is much more intense than the higher energy PA band. This is very good for laser action applications obtained with carrier injection, since in this case the high energy PA band of the injected DP excitations cannot compete with the PL band. Unfortunately, however, the PL of this material is very low and there is no SE in the ps time domain.

Since the DP relaxation energy is very low, there is overlap between the electronic and vibrational bands that leads to quantum interference between a group of strongly coupled photoinduced phonons and the lower energy polaron band in the photoinduced absorption spectrum. This phenomenon also occurs in several other ordered π-conjugated polymer films, where the lower energy polaron PA band appears at very low energy due to small polaron relaxation energy. The Fano-like interference leads to anti-resonances superimposed on the lower energy polaron PA band, which appears due to the frequency overlap between the lower polaron band and the photoinduced IRAVs in these materials. An excellent quantitative agreement between the experimental data and a theoretical model calculation using the AM model and CDW conductivity band, leads us to infer the existence of a continuum band in the charge manifold of these ordered polymer films.

Experimental

In our optical measurements we have used both fs transient as well as steady state spectroscopies.

FS Spectroscopies: In the ps time-resolved measurements the short pump pulse creates photoexcitations in the film and a time-delayed probe pulse measures the resulting change in transmission as a function of the pump-probe delay time. We used pulses from an amplified Ti:sapphire laser system operating at a repetition rate of 1 kHz. Pulses 50 fs in duration centered at 800 nm were doubled into the UV (400 nm, or 3.1 eV) using second harmonic generation in a BBO crystal. Probe pulses of variable wavelength were produced by using a portion of the amplified 800 nm beam to generate a femtosecond white light supercontinuum in a 1 mm thick sapphire plate. Wavelength resolution of about 6 nm in the probe beam was achieved by a 0.3 met monochromator having a 200 μm exit slit, that was placed in the probe beam after it had passed through the film. The pump beam was modulated mechanically at exactly half the repetition rate of the Ti:sapphire laser system (≈ 500 Hz) [8,14], and the resulting change, ΔI in the probe beam energy, I was detected with phase sensitive technique using lock-in amplification. Our ps spectrometer had about 100 fs time resolution with measurements sensitivity, $\Delta I/I \approx 10^{-4}$.

For the present studies all measurements were carried out at room temperature in a cryostat providing a dynamical vacuum of 100 μtorr to prevent the polymer degradation with strong laser illumination at ambient conditions [15]. We used the time-resolved differential transmittance technique with time delays ranging from 100 fs to 200 ps. For each sample film, measurements were carried out over a range of pump fluences that correspond to a range of initial photoexcitation densities from 5×10^{17} to 10^{19} cm^{-3}. Photoexcitations resulted in PA, which is represented in the spectra as negative differential transmittance, $-\Delta T/T$, where ΔT is the change in transmittance, T due to the action of the pump pulse. Pump induced SE and photobleaching (PB) of the optical absorption in the ground state with $\Delta T > 0$ were also measured. In the small signal limit, $\Delta T(t)$ is expected to be proportional to the photoexcitation density, $N(t)$, which for an optically thick film is given by the relation: $\Delta T/T = N\sigma\alpha_L$, where σ is the photoexcitation optical cross section of and α_L is the absorption coefficient at the laser excitation wavelength.

Steady State Spectroscopies: For the cw PA measurements we used a standard photomodulation (PM) set-up as well as a modified Fourier transform IR (FTIR) spectrometer at 10 K. In the PM technique the spectrum of $\Delta T/T$ is measured in a much broader spectral range than in the ps time domain. We utilize a number of solid state detectors, a lock in amplifier referenced to a modulated cw Ar^+ laser beam used for excitation, and a dispersed beam from an incandescent light source

  1616-301X/02/0909-0596 $ 17.50+.50/0

ADVANCED FUNCTIONAL MATERIALS

as a probe. The PL spectrum is recorded without the probe beam on the sample in order to eliminate pump-related emission that interferes with the ΔT measurements. For the PM using the FTIR we measured the sample transmission with very high accuracy (approximately 5000 scans) in a broad spectral range of 100 to 5000 cm^{-1} in the dark, and when the sample was illuminated with an Ar^+ laser. The modulated $\Delta T/T$ spectrum was then calculated with a sensitivity of 10^{-5}. For the PM measurements at high pressure a high-pressure diamond anvil cell was introduced into the sample chambre of the FTIR; the high pressures were calibrated using the shifts of the IR-active C–H vibration frequencies with pressure.

Usually a variety of photoexcitations contribute to the $\Delta T/T$ spectrum, and therefore we have to use other means to separate their contributions in the PM spectrum. For example we have applied the PADMR spectroscopy [50] to separate the various photoexcitations contributions according to their spin-related recombination kinetics. This is usually related to the photoexcitations spin-state. In this way we could separate spin 1 from spin 1/2, and spin 0 photoexcitations in the PA spectra. For the PADMR spectroscopy [50] the sample was mounted in a high Q microwave cavity at 3 GHz equipped with a superconducting magnet and illuminated by the cw pump and probe beams and the microwaves. We measured the H-PADMR spectrum, in which the resonance-related changes, ΔT in T is monitored at a fixed probe wavelength, λ as the magnetic field, H is varied, as well as the λ-PADMR spectrum where ΔT is measured at a fixed magnetic field, while the probe beam is varied.

Sample Preparation: The samples were thin films of RR-P3HT (92 % RR regio-order, M_w of 28 kg/mol) that were grown in our laboratory as well as RR-P3HT and RRa-P3HT that were purchased from Aldrich [51]. The films were cast from different solutions such as chloroform, benzene, and xylene (usually at a concentration of a few $mg\,mL^{-1}$) onto sapphire or quartz substrates. Special care was taken to minimize contamination of the powders and films by oxygen and water at ambient conditions.

Received: May 27, 2002

[1] J. Cornil, D. Beljonne, J. P. Calbert, J.-L. Brédas, *Adv. Mater*. **2001**, *13*, 1053.
[2] G. Horowitz, *Adv. Mater*. **1998**, *10*, 365.
[3] H. Sirringhaus, P. J. Brown, R. H. Friend, M. M. Nielsen, K. Bechgaard, B. M. W. Langeveld-Voss, A. J. H. Spiering, R. A. J. Janssen, E. W. Meijer, P. Herweg, D. M. de Leeuw, *Nature* **1999**, *401*, 685.
[4] H. Sirringhaus, N. Tessler, R. H. Friend, *Science* **1998**, *280*, 1741.
[5] J. H. Schön, A. Dodabalapur, Z. Bao, C. Kloc, B. Batlogg, *Nature* **2001**, *410*, 189.
[6] P. J. Brown, H. Sirringhaus, M. Harrison, M Shkunov, R. H. Friend, *Phys. Rev. B* **2001**, *63*, 125 204.
[7] R. Österbacka, C. P. An, X. M. Jiang, Z. V. Vardeny, *Science* **2000**, *287*, 839.
[8] O. J. Korovyanko, R. Österbacka, X. M. Jiang, Z. V. Vardeny, R. A. J. Janssen, *Phys. Rev. B* **2001**, *64*, 235 122.
[9] S. V. Frolov, M. Liess, P. A. Lane, W. Gellermann, Z. V. Vardeny, M. Ozaki, K. Yoshino, *Phys. Rev. Lett.* **1997**, *78*, 4285.
[10] a) V. I. Klimov, D. W. McBranch, N. Barashkov, J. Ferraris, *Phys. Rev. B* **1998**, *58*, 7654. b) B. Kraabel, V. I. Klimov, R. Kohlman, S. Xu, H. L. Wang, D. W. McBranch, *Phys. Rev. B* **2000**, *61*, 8501.
[11] a) V. I. Klimov, D. W. McBranch, *Chem. Phys. Lett*. **1997**, *277*, 109. b) M. A. Stevens, C. Silva, D. M. Russell, R. H. Friend, *Phys. Rev. B* **2001**, *63*, 165213.
[12] A. Dogariu, A. J. Heeger, H. Wang, *Phys. Rev. B* **2000**, *61*, 16 183.
[13] O. J. Korovyanko, G. A. Levina, Z. V. Vardeny, *Synth. Met*. **2001**, *119*, 631.
[14] V. I. Klimov, D. W. McBranch, *Opt. Lett*. **1998**, *23*, 277.
[15] a) M. Yan, L. J. Rothberg, F. Papadimitrakopoulos, M. E. Galvin, T. M. Miller, N. N. Barashfov, J. P. Ferraris, *Phys. Rev. Lett*. **1994**, *72*, 1104. b) M. Yan, L. J. Rothberg, E. W. Kwock, T. M. Miller, *Phys. Rev. Lett*. **1995**, *75*, 1992.
[16] G. Rumbles, I. D. W. Samuel, C. J. Collison, P. F. Miller, S. C. Moratti, A. B. Holmes, *Synth. Met*. **1999**, *101*, 158.
[17] D. Beljonne, J. Cornil, H. Sirringhaus, P. J. Brown, M. Shkunov, R. H. Friend, J.-L. Brédas, *Adv. Funct. Mater*. **2001**, *11*, 229.
[18] Other mechanisms, such as exciton migration to the longest chain outside the lamellae structures may also contribute to the apparent PL Stokes shift.
[19] S. V. Frolov, Z. Bao, M. Wohlgenannt, Z. V. Vardeny, *Phys. Rev. Lett*. **2000**, *85*, 2196.
[20] D. Hu, J. Yu, K. Wong, B. Bagchi, P. J. Rossky, P. F. Barbara, *Nature* **2000**, *405*, 1030.
[21] a) U. Mizrahi, D. Gershoni, E. Ehrenfreund, Z. V. Vardeny, *Synth. Met*. **1999**, *102*, 1182. b) U. Mizrahi, D. Gershoni, E. Ehrenfreund, Z. V. Vardeny, *Synth. Met*. **2001**, *119*, 507.
[22] a) D. Moses, A. Dogariu, A. J. Heeger, *Chem. Phys. Lett*. **2000**, *316*, 356. b) D. Moses, A. Dogariu, A. J. Heeger, *Phys. Rev. B* **2000**, *61*, 9373.
[23] A. Dogariu, D. Vacar, A. J. Heeger, *Phys. Rev. B* **1998**, *58*, 10 218.
[24] a) Z. V. Vardeny, J. Strait, D. Moses, T. C. Chung, A. J. Heeger, *Phys. Rev. Lett*. **1982**, *49*, 1657. b) C. V. Shank, R. Yen, R. L. Fork, J. Orenstein, G. L. Baker, *Phys. Rev. Lett.* **1982**, *49*, 1660.
[25] R. Österbacka, M. Wohlgenannt, D. Chinn, Z. V. Vardeny, *Phys. Rev. B* **1999**, *60*, R11 253.
[26] R. Österbacka, C. P. An, X. M. Jiang, Z. V. Vardeny, *Synth. Met.* **2001**, *116*, 317.
[27] B. Kraabel, D. Moses, A. J. Heeger, *J. Chem. Phys.* **1995**, *103*, 5102.
[28] J. J. Apperloo, R. A. J. Janssen, P. R. L. Malenfant, J. M. J. Fréchet, *J. Am. Chem. Soc.* **2001**, *123*, 6916.
[29] K. Fesser, A. Bishop, D. K. Campbell, *Phys. Rev. B* **1983**, *27*, 4804.
[30] R. Österbacka, X. M. Jiang, C. P. An, B. Horovitz, Z. V. Vardeny, *Phys. Rev. Lett.* **2002**, *88*, 226 401.
[31] X. M. Jiang, C. P. An, R. Österbacka, Z. V. Vardeny, *Synth. Met.* **2001**, *116*, 203.
[32] Z. Bao, A. Dodabalapur, A. J. Lovinger, *Appl. Phys. Lett.* **1996**, *69*, 4108.
[33] T. Nguyen, I. B. Martini, J. Liu, B. J. Schwartz, *J. Phys. Chem. B* **2000**, *104*, 237.
[34] a) F. L. Pratt, K. S. Wong, W. Hayes, D. Bloor, *J. Phys. C* **1987**, *20*, L41. b) F. L. Pratt, K. S. Wong, W. Hayes, D. Bloor, *J. Phys. D* **1987**, *20*, 1361.
[35] Y. H. Kim, D. Spiegel, S. Hotta, A. J. Heeger, *Phys. Rev. B* **1988**, *38*, 5490.
[36] B. Horovitz, *Solid State Commun.* **1982**, *41*, 729.
[37] E. Ehrenfreund, Z. V. Vardeny, O. Brafman, B. Horovitz, *Phys. Rev. B* **1987**, *36*, 1535.
[38] U. Fano, *Phys. Rev.* **1961**, *124*, 1866.
[39] F. Cerdeira, T. A. Fjeldly, M. Cardona, *Phys. Rev. B* **1973**, *8*, 4734.
[40] M. V. Klein, in *Light Scattering in Solids* (Ed: M. Cardona), Springer, Heidelberg **1983**, p. 147.
[41] S. Glutsch, U. Siegner, M. A. Mycek, D. S. Chemla, *Phys. Rev. B* **1994**, *50*, 17009.
[42] V. I. Belitsky, A. Cantarero, M. Cardona, C. Trallero-Giner, S. T. Pavlov, *J. Phys., Condens. Matter* **1997**, *9*, 5965.
[43] M. J. Rice, *Phys. Rev. Lett.* **1976**, *37*, 36.
[44] B. Horovitz, H. Gutfreund, M. Weger, *Phys. Rev. B* **1978**, *17*, 2796.
[45] The CDW response function is given for $\omega < 2\Delta$ by $f(\omega) = (4\Delta^2/\omega^2 y)\arctan(1/y)$; whereas for $\omega > 2\Delta$, $f(\omega) = (2\Delta^2/\omega^2 y)\{\ln[(1-y)/(1+y)] + \pi i\}$, where $y = (1-4\Delta^2/\omega^2)^{1/2}$. The CDW gap is 2Δ that is also equal to E_r.
[46] Most of the RR-P3HT bare frequencies, ω_n are very close to those of the obtained ARs (Fig. 7a), with an average normalized coupling constant $\lambda_n/\lambda = 0.007$. In contrast, the five most important modes have the following bare frequencies and couplings:[30] $\omega_{10} = 1237\ cm^{-1}$, $\lambda_{10}/\lambda = 0.019$; $\omega_4 = 745\ cm^{-1}$, $\lambda_4/\lambda = 0.024$; $\omega_6 = 890\ cm^{-1}$, $\lambda_6/\lambda = 0.014$; $\omega_7 = 1020\ cm^{-1}$, $\lambda_7/\lambda = 0.011$; $\omega_{10} = 1237\ cm^{-1}$, $\lambda_{10}/\lambda = 0.019$; $\omega_{13} = 1996\ cm^{-1}$, $\lambda_{13}/\lambda = 0.876$.
[47] L. Sebastian, G. Wiser, *Phys. Rev. Lett.* **1981**, *46*, 1156.
[48] I. G. Hill, A. Kahn, Z. G. Soos, R. A. Pascal, Jr, *Chem. Phys. Lett.* **2000**, *327*, 181.
[49] R. H. Friend, R. W. Gymer, A. B. Holmes, J. H. Burroughes, R. N. Marks, C. Taliani, D. D. C. Bradley, D. A. dos Santos, J.-L. Brédas, M. Lögdlund, W. R. Salaneck, *Nature* **1999**, *397*, 121.
[50] Z. V. Vardeny, X. Wei, in *Handbook of Conducting Polymers* (Eds: T. A. Skotheim, R. Elsenbaumer, J. R. Reynolds), 2nd ed., Marcel Dekker, New York **1997**.
[51] Aldrich Chemical Company, Milwaukee, Wisconsin (USA).

  1616-301X/02/0909-0597 $ 17.50+.50/0